# Supplementary Information

## Electrodeposited films to MOF-derived electrochemical energy storage electrodes: a concept of simplified additive-free electrode processing for self-standing, ready-to-use materials

Julia Linnemann,*[a,b] Laura Taudien,[a,b] Markus Klose,[a] and Lars Giebeler[a]

[a.] *Leibniz-Institute for Solid State and Materials Research (IFW) Dresden e.V., Institute for Complex Materials, Helmholtzstr. 20, D-01069 Dresden, Germany*
*E-mail: j.linnemann@ifw-dresden.de; linnemannjulia@gmail.com*
[b.] *Technische Universität Dresden, Physical Chemistry, Bergstr. 66b, D-01069 Dresden, Germany*

## Experimental

### Materials

Metal-organic framework films were electrodeposited on 0.125 mm thick cobalt foil (99.9 %, Goodfellow) and 0.05 mm thick stainless steel foil (M-Tech). The respective electrolyte solutions were prepared with 1,3,5-benzenetricarboxylic acid ($H_3BTC$, 95 %, Sigma-Aldrich), methyl-tributyl-ammonium methylsulfate (MTBS, ≥ 95 %, Sigma-Aldrich), 2-methylimidazol (≥ 99 %, Merck), manganese(II) sulfate monohydrate ($MnSO_4 \cdot H_2O$, analytical grade, Merck), sodium nitrate ($NaNO_3$, ≥ 99.5 %, Merck) and ethanol (absolute, analytical grade, Merck). For powder electrode formulations, polyvinyliden difluoride (PVDF-21216, Solvay) was used as binder and N-methyl-2-pyrrolidone (NMP, ≥ 99 %, VWR) as solvent.

### Electrochemical MOF film synthesis

Metal foils were cleaned with deionised water and ethanol before they were pressed on O-rings and assembled in an electrochemical Teflon synthesis cell. A circular area of a metal foil with a diameter of 10 mm is exposed to the electrolyte solution. The deposition experiments were performed in three electrode configuration with a platinum counter electrode and a mercury sulfate reference electrode which was connected to the cell by a salt bridge. A Heka PG310 potentiostat was used for $[Co_3(BTC)_2(H_2O)_{12}]$ (Co-BTC) films and coating of Mn/Mn-BTC was performed with a Methrom Autolab PGSTAT204 potentiostat.

#### Co-BTC films on cobalt foil

The Co-BTC films were deposited potentiostatically on cobalt foil with an 3:1 (v/v) ethanol-water-based electrolyte solution containing 0.05 mol $l^{-1}$ 1,3,5-benzenetricarboxylic acid ($H_3BTC$) and 0.05 mol $l^{-1}$

$NaNO_3$. At 0.5 V *vs.* MSE, Co foils were anodically dissolved for 1 h at room temperature. The colour of the electrolyte solution became pink indicating that a significant amount of the produced $Co^{2+}$ cations was not incorporated into the metal-organic coating.

Several other procedures were conducted to develop the synthesis protocol for Co-BTC films suitable for thermolysis to electrochemical active coatings. Parameters of those which are relevant to the discussion are summarised in ESI-Table 1.

**ESI-Table 1.** Selection of further experimental parameters evaluated to develop an electrochemical coating procedure to obtain high-quality Co-BTC framework films.

| Electrolyte | Polarisation method | Duration |
|---|---|---|
| 0.05 mol $l^{-1}$ $H_3BTC$<br>0.06 mol $l^{-1}$ MTBS<br>3:1 ethanol/water | potentiostatic<br>0.1 V - 1 V *vs.* MSE | 5 min - 240 min |
| 0.05 mol $l^{-1}$ $H_3BTC$<br>3:1 ethanol/water | potentiostatic<br>0.5 V *vs.* MSE | 90 min |
| 0.05 mol $l^{-1}$ $H_3BTC$<br>3:1 ethanol/water | pulse-current<br>0.637 mA $cm^{-2}$ pulse-current density, 0.5 Hz, square wave | 90 min |

### Mn/Mn-BTC bilayered films on stainless steel foil

At first, manganese was electrodeposited on stainless steel foils from aqueous 0.1 M $MnSO_4$ electrolyte solution. A potential of -2 V *vs.* MSE was applied for 30 min. Here, a stainless steel counter electrode was used. After removing the electrolyte, the manganese film was rinsed several times with water and then immediately converted to the metal-organic coating. Freshly prepared Mn films were anodically dissolved in a 1:1 (v/v) ethanol/water mixture with 0.05 mol $l^{-1}$ 1,3,5-benzenetricarboxylic acid and 0.025 mol $l^{-1}$ 2-methylimidazol as directing agent by applying -1.25 V *vs.* MSE for 1 h.

## Electrochemical Co-BTC powder synthesis

The electrochemical synthesis of Co-BTC as powder was performed galvanostatically (0.065 A) under stirring for 4 h at room temperature in two electrode configuration with a platinum counter electrode. A Co foil was applied as working electrode, of which 2.3 x 2.8 $cm^2$ (each side) were exposed to the electrolyte (60 ml) containing 0.05 M $H_3BTC$ and 0.06 M methyl-tributylammonium methylsulfate (MTBS) in a 3:1 (v/v) ethanol/water mixture. From the beginning of the synthesis process, the colour of the colourless electrolyte solution changed continuously to pink, which corresponds to the increasing concentration of $Co^{2+}$ cations. The solution remained clear until flocculation started after ca. 30 min. After finishing the polarisation, 890 mg of a pale rose precipitate were filtered, washed with ethanol and water, and dried under ambient conditions. The yield was determined to be 67 % based on the amount of $cobalt^{(II)}$ cations released into the electrolyte solution, which was calculated according to Faraday's law assuming a current efficiency of 100 %. The product was identified as the

metal-organic framework [$Co_3(BTC)_2(H_2O)_{12}$] by powder X-Ray diffraction (XRD) and comparison to a pattern calculated from CCDC-1274034.

## Thermolyses of metal-organic films and powders

To convert electrochemically deposited metal-organic films to metal oxide/carbon hybrid films, they were thermally treated with a tube furnace under argon atmosphere (flow rate = 0.2 $l_n$ $min^{-1}$). Coated Co foils were heated up to 800 °C within 3 h and kept at this temperature for 1 h. After cooling down to room temperature, the coated foils were returned to air. Steel foils with Mn/Mn-BTC bilayered coatings were thermolysed at 500 °C for 1 h applying a heating rate of 300 K $h^{-1}$. For comparison of the electrochemical properties, uncoated metal foils were also annealed under the same conditions as the respective coated foils.

500 mg Co-BTC powder was placed in a ceramic vessel and pyrolysed like Co-BTC films (800 °C, 1 h).

The phases of the resulting materials were identified by XRD in comparison to published data: PDF# 01-071-1178 (CoO), PDF# 01-078-1970 ($Co_3O_4$), PDF# 01-075-1621 (C, graphite), PDF# 01-088-2325 ($\beta$-Co), PDF# 01-080-0382 ($Mn_3O_4$), PDF# 01-086-0666 ($\delta$-$MnO_2$).

## Film and powder characterisation

X-ray diffraction (XRD) measurements on the metal-organic and thereof derived films as well as metal foils were conducted in reflection mode with a Philips 1050 Diffractometer using Co K$\alpha$ radiation ($\lambda$ = 1.790307 Å). Signals of the underlying foil substrates were also observed as the film thickness is limited. The chosen measurement range for Co-BTC films avoids the main reflections of the cobalt substrates but allows for checking phases with reflections < 45 ° 2θ. Powder samples were characterised in transmission mode with a STOE STADI P powder diffractometer using Co-K$\alpha_1$ radiation ($\lambda$ = 1.78896 Å).

The optical microscope Zeiss Axioskop 40 was used to evaluate the quality of the electrodeposited films, in respect of the density and homogeneity of the crystal coatings. Morphologies of film and powder samples were further investigated by scanning electron microscopy with a FEG Gemini Leo 1530 from Zeiss. The energy dispersive X-Ray spectrometer Bruker XFlash Detector 4010, applied to characterise the composition of the thermolysed metal-organic materials, was connected to the microscope.

Thermal analysis of the [$Co_3(BTC)_2(H_2O)_{12}$] powder was performed under argon atmosphere with a Netzsch STA 449C Jupiter device applying a heating rate of 5 K $min^{-1}$ and connected to a Pfeiffer Vacuum Prisma quadrupole mass spectrometer.

The electrochemical properties of thermolysed samples were investigated in a three electrode Teflon cell setup with a platinum counter electrode and a mercury sulfate reference electrode (MSE). Cyclic voltammograms (CVs) were measured in different potential ranges and at various scan rates, ranging from 2 mV $s^{-1}$ to 20 mV $s^{-1}$, to examine electrochemical processes related to energy storage properties in detail.

Thermolysed Co-BTC films on Co foil and thermolysed Co foil were cycled in aqueous 0.5 M KOH solution using a Heka PG310 potentiostat. At first, a wide potential range (-1.3 V to 0.1 V *vs.* MSE) was used at a scan rate of 2 mV $s^{-1}$ to observe the initial electrochemical properties of thermolysed films

and to identify the potential range where a pseudocapacitive current signature is observed. The amount of energy stored in a capacitor electrode depends on the square of the potential window. Therefore, it is of interest to investigate the widest possible operating potential window of a pseudocapacitive electrode material. In some experiments, potentials ≥ 0.1 V *vs.* MSE were also used as positive reverse potential. In this case, the onset current of the oxygen evolution reaction was observed. In consideration of the CVs recorded in the wide potential windows, a potential range from -0.6 V to 0.1 V *vs.* MSE was used for further measurements to investigate the pseudocapacitive properties of the system.

Thermolysed Mn/Mn-BTC bilayered films and annealed stainless steel foil were cycled in aqueous 0.5 M $K_2SO_4$ solution with a pH value of 10 using a Methrom Autolab PGSTAT204 potentiostat. The electrolyte composition was chosen according to the electrochemical properties of manganese oxides in aqueous $K_2SO_4$ solution and the pH stability range of manganese oxide species.[1] Thermolysed Mn/Mn-BTC films exhibited a redox-current signature over a wide potential window from -1.6 V to 0.85 V *vs.* MSE. For even wider potential windows, onset signals of hydrogen or oxygen evolution were observed indicating electrolyte decomposition.

Three samples of thermolysed Mn/Mn-BTC bilayered films were dissolved in nictric acid and hydrochloric acid to determine the manganese content by inductively coupled plasma optical emission spectrometry (ICP-OES) and to calculate the corresponding amount of $Mn_3O_4$. The calculation of gravimetric capacitances in F $g^{-1}$ refers to this amount of $Mn_3O_4$. As the obtained values for the manganese content were close to each other, the average amount of 0.73 mg $cm^{-2}$ was used to calculate the corresponding $Mn_3O_4$ loading (1.0 mg $cm^{-2}$).

Potentiostatic electrochemical impedance spectroscopy (EIS) measurements were conducted with an AC amplitude of ± 10 mV in a frequency range from 10 kHz to 1 Hz using a Methrom Autolab PGSTAT204 instrument with a FRA32M module. The EIS data were obtained at the open circuit potentials (OCPs), observed after 20 min of relaxation time following cyclic voltammetry measurements, and at potentials corresponding to significant features in the respective CVs. The potential of a capacitor electrode is related to the state of charge of a capacitor device. The respective electrode potentials were adjusted at a sweep rate of 20 mV $s^{-1}$. A Co-BTC film-derived electrode was characterised in 0.5 M KOH at the OCP (-0.482 V *vs.* MSE), the A1 peak potential (-0.275 V *vs.* MSE), a potential in the current plateau region (-0.115 V *vs.* MSE) and at the positive reverse potential corresponding to the A2 peak potential (0.100 V *vs.* MSE). A Co-BTC powder-derived electrode was also characterised in 0.5 M KOH at the relevant potentials: -0.340 V, -0.135 V, -0.09 V and 0.04 V *vs.* MSE. Impedance spectra of a Mn/Mn-BTC-derived electrode were measured in 0.5 M $K_2SO_4$ with a pH value of 10 at the OCP (-0.375 V *vs.* MSE), the A1 peak potential (-0.250 V *vs.* MSE), the A2 peak potential (0.300 V vs. MSE) and at the A3 peak potential (0.800 V *vs.* MSE). The linear Kramers-Kronig test implemented in Methrom Autolab Nova 1.1 software was used to validate the obtained impedance data.

For powder electrode preparation, a mixture of thermolysed Co-BTC powder and polyvinyliden difluoride (PVDF-21216) as binder in N-methyl-2-pyrrolidone (NMP) was homogenized by a Retsch MM 200 shaker and then doctor bladed on stainless steel foil. Steel foil was chosen because it is a typical

and inexpensive current collector material often applied in powder electrode studies. The concentration of the slurry was 100 mg (95 % Co/C material, 5 % binder) per 300 µl NMP. After drying at 55 °C, the electrodes were characterized under similar conditions as the Co-BTC film-derived samples. The initial cyclic voltammetry at 2 mV $s^{-1}$ in a potential range from -1.5 V to 0.04 V *vs.* MSE was also used as a primary oxidation treatment to convert the cobalt particles in the carbon matrix to pseudocapacitively active $Co_3O_4$. In regard of the CVs recorded in the wide potential windows, the potential range for further cyclic voltammetry measurements was limited to -0.5 V – 0.04 V *vs.* MSE.

## Determination of electrochemical capacitance and capacity values

In general, there are two ways to define the term capacitance in an electrochemical context: integrally or differentially. The quantity integral capacitance $C_{int}$ accounts commonly for the analogy of the electrochemical double layer of an electrode and a plate capacitor. It describes the electrochemical capacitance according to equation (1) as sum of accumulated excess charges at the solution interface in relation to the potential difference $\Delta E$ of the electrode and the solution (Galvani potential).[2,3] The charge $Q$ is equivalent to the integral amount of current passed into the double layer electrode over time.

$$C_{int} = \frac{Q}{\Delta E} = \frac{\int I dt}{\Delta E} \qquad (1)$$

The process of charging (and discharging) can also be expressed with a differential coefficient referred to as differential capacitance $C_{dif}$. It is often a more suitable quantity to describe electrochemically capacitive systems as the change of the charge corresponding to a certain change of the potential may depend on the initial potential.[3]

$$C_{dif} = \frac{dQ}{dE} \qquad (2)$$

As shown in equation (3), the values of the differential and the integral capacitance of an electrode are equal only if the differential capacitance is independent of the potential.[2,4]

$$C_{dif} = C_{int} + \Delta E \frac{dC_{int}}{dE} = C_{int} + \Delta E \frac{d\left(\frac{Q}{\Delta E}\right)}{dE} \qquad (3)$$

The current transients in ESI-scheme 1 demonstrate the significance of this issue for cyclic voltammetry characterisation of electrochemical capacitor electrodes. In the ideal case, when the current is constant over the whole potential range, the differential capacitance at any potential equals the integral capacitance over the whole potential range. If the current varies with respect to the potential, the value of an integral capacitance calculated for the whole measured potential range overestimates the actual (differential) capacitance in the plateau region of constant current and underestimates it in the peak region.

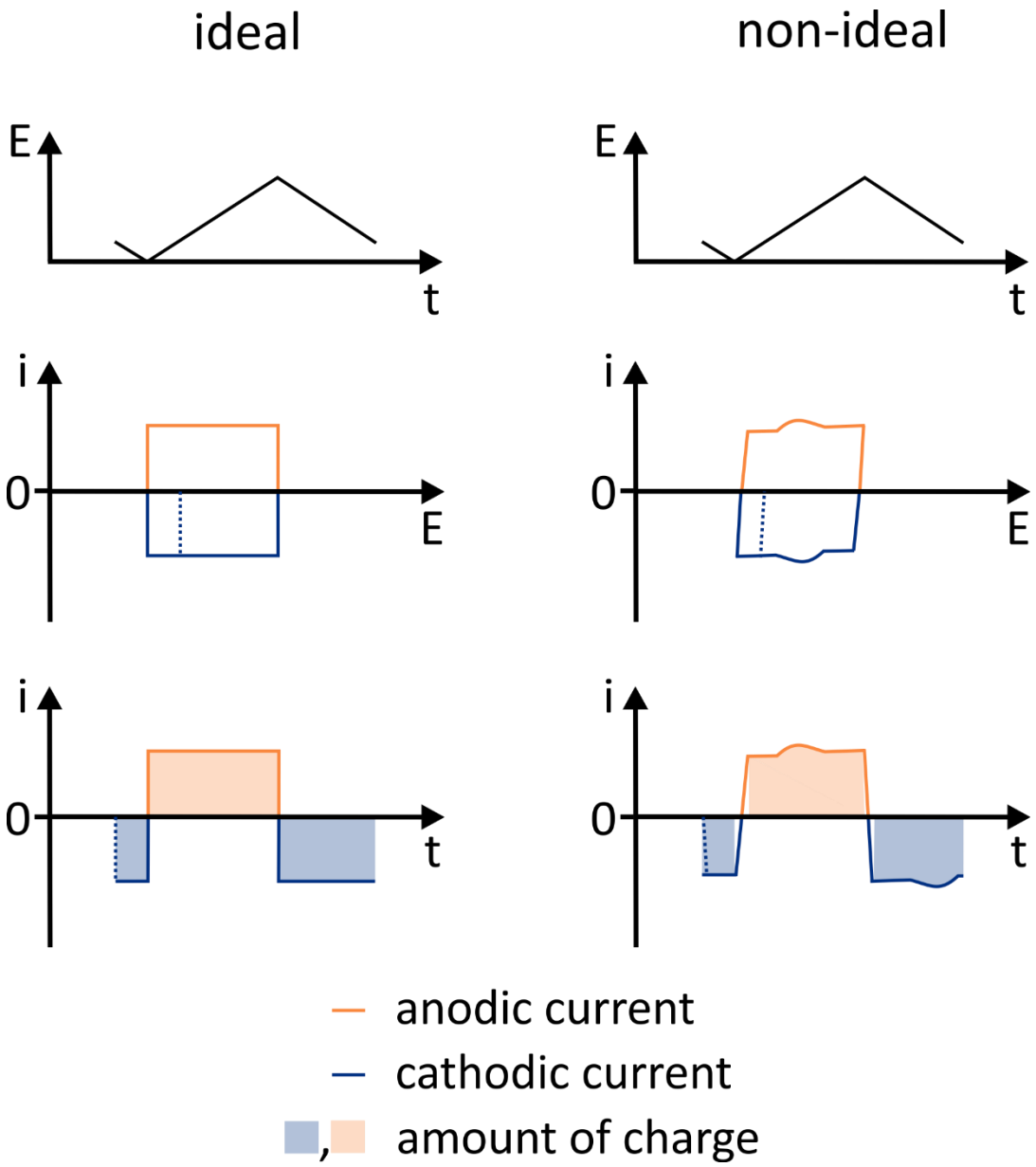


**ESI-Scheme 1.** Potential (*E*) - time (*t*) transients and current density (*i*) transients of cyclic voltammetry measurements with electrochemical capacitive electrodes.

Besides electrochemical double layer capacitance which is based on electrostatic charge separation, capacitive behaviour may arise due to fast, reversible faradaic processes occuring at the electrode surface. They cause a reaction quantity whose derivative with respect to the potential has the dimension of a capacitance. This quantity is termed pseudocapacitance. For example, such a pseudocapacitance can be deduced for electrochemical redox processes from the Nernst equation.[5]
The differential capacitance $C_{dif}$ of an electrode material in relation to the electrode potential can be determined by cyclic voltammetry in a three electrode configuration considering relationship (4). There $I$ is the current, $Q$ the charge, $t$ the time and $E$ the electrode potential.[3,4] As demonstrated by equation (5), values of differential capacitances $c_{dif}$ for Co-BTC-derived materials were calculated from measurements with different scan rates $v$ evaluating the current densities $i$ at different potentials. The

respective potentials are the peak potential of the $Co^{(II)}/Co^{(III)}$ transition, -0.115 V *vs.* MSE (within the range where a current plateau was observed) and near the positive reverse potential.

$$I(E) = \frac{\partial Q(E)}{\partial t} = \frac{\partial Q(E)}{\partial E} \cdot \frac{dE}{dt} = C_{dif}(E) \cdot \frac{dE}{dt} \quad (4)$$

$$c_{dif}(E) = \frac{i(E)}{\frac{dE}{dt}} = \frac{i(E)}{\nu} \quad (5)$$

As pseudocapacitance is a property of a material and not of a capacitor device,[4,6] the characterization measurements are conducted against a reference electrode. The performance of the material can be different in a two electrode test cell or in an actual supercapacitor depending on the material of the second electrode. It would be lowered if only a part of the potential range (referring to the single electrode against a reference electrode) is used. For example, this is the case in a symmetric capacitor applying the same active material for both electrodes. However, in so-called asymmetric or hybrid capacitors, a complementary potential range can be used by appropriate selection of the second electrode material.[6] Therefore, characterisation in three electrode configuration allows not only for more detailed investigation of the electrochemical properties regarding underlying mechanisms and kinetics, but also for gaining information on how to design a capacitor device with higher performance through well-matched electrode materials. Moreover, hybrid supercapacitors can be made of an electrochemical capacitive electrode (double-layer- or pseudocapacitive) and a high-rate capable faradaic electrode. The electrical signature of these devices are then similar to those of capacitors because of the capacitive nature of one electrode, even if the other one does not have capacitive properties.[6]

As electrochemical redox reactions are involved in the charge storage mechanism of the metal oxide/carbon hybrid films in this study, the physical meaning of integral capacitance values (in the form of whole amount of charge divided by the whole potential range) is questionable. This is especially the case for $Mn_3O_4$ materials where capacitive behaviour is not observed over the complete range. Nevertheless, to enable better comparability to other work, we calculated integral capacitances by integrating current-density time graphs with Origin 2015G software to determine anodic and cathodic charges and dividing them by the respective potential range according to equation (1). The calculated charges were also analysed with regard to the balance of anodic and cathodic processes. They can be considered as capacities, which is a more appropriate physical quantity to describe faradaic charge storage that does not cause a capacitive-like electrochemical signature. The cyclic voltammogram (CV) of an ideal electrochemical capacitor electrode has a rectangular shape with an immediate current response when changing the scanning direction as well as balanced anodic and cathodic charges.[7,8] As ESI-Scheme 1 demonstrates, for non-ideal systems, there may be a short time interval for the switching from anodic to cathodic current and vice versa. Thus, the integration limits were set from the time when the current had the appropriate sign until the time when the reverse potential was reached. The charge excluded by this procedure does not contribute to the energy storage performance of a device, hence, its exclusion is appropriate.

## Images and XRD data of further electrodeposited Co-BTC films

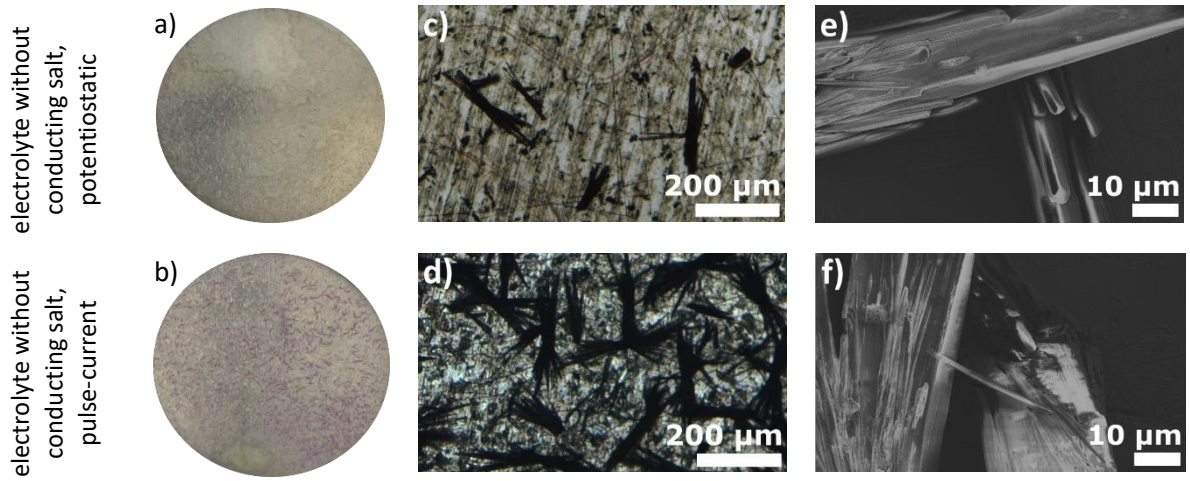


**ESI-Fig. 1** (a, b) Photographs, (c, d) optical micrographs and (e, f) scanning electron micrographs of Co-BTC films electrodeposited potentiostatically (top row: a, c, e) or with pulse-current (bottom row: b, d, f) with an electrolyte (0.05 mol $l^{-1}$ $H_3BTC$ in 3:1 ethanol/water solution) not containing a conducting additive.

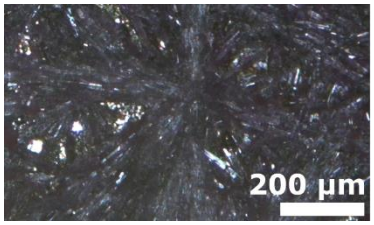


**ESI-Fig. 2** For comparison: optical micrograph of a Co-BTC film deposited potentiostatically with an electrolyte containing 0.05 mol $l^{-1}$ $NaNO_3$ as conducting salt, of the kind which was thermolysed and presented in detail in the main article.

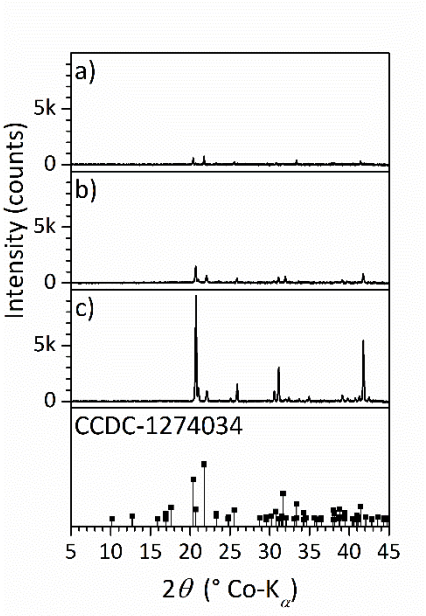


**ESI-Fig. 3** XRD patterns of Co-BTC films on Co foil electrodeposited (a) potentiostatically or (b) with pulse-current with an electrolyte (0.05 mol $l^{-1}$ $H_3BTC$ in 3:1 ethanol/water solution) not containing a conducting additive or (c) potentiostatically with an electrolyte containing 0.05 mol $l^{-1}$ $NaNO_3$ as conducting salt, of the kind which was thermolysed and presented in detail in the main article.

## EDXS measurements on thermolysed MOF films

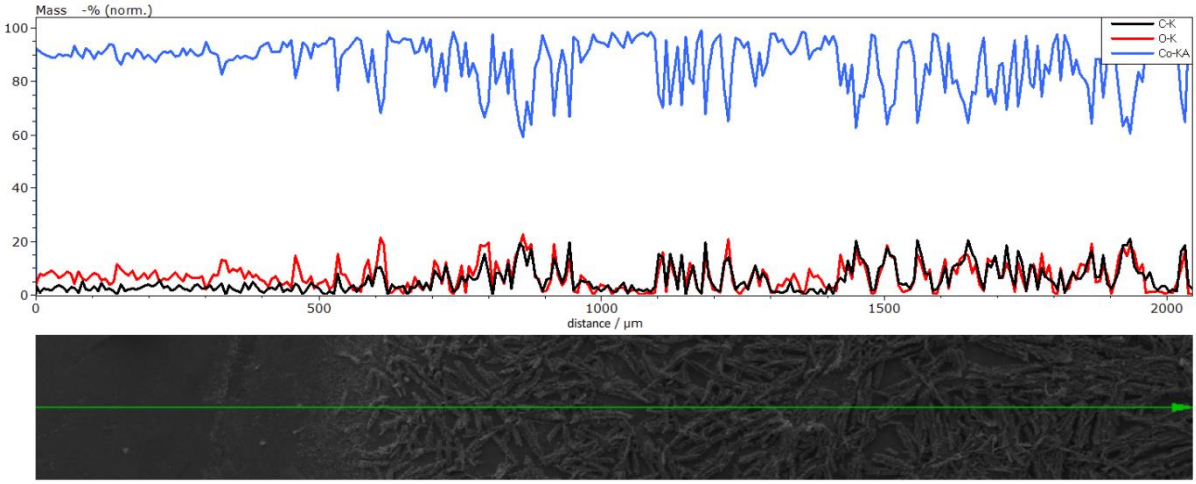


**ESI-Fig. 4** Quantitative representation of an EDXS line scan of the edge of an electrodeposited Co-BTC film and the underlying Co foil showing carbon (black), oxygen (red) and cobalt (blue) content in normalized wt.%.

**ESI-Table 2** Carbon content of thermolysed metal-organic films at different positions on the derived structures and of the metal foil substrates as determined by EDXS measurements.

| Measurement position | Carbon content of thermolysed Co-BTC film (wt.%) | Carbon content of thermolysed Mn-BTC film (wt.%) |
|---|---|---|
| MOF-derived structure I | 12.11 | 18.19 |
| MOF-derived structure II | 15.07 | 16.96 |
| MOF-derived structure III | 13.33 | 17.95 |
| Substrate | 3.16 | 2.89 |

## EDXS measurements on thermolysed Co-BTC powder

**ESI-Table 3** Composition of thermolysed Co-BTC powder particles determined by several EDXS measurements at different positions.

| Measurement | Cobalt content (wt.%) | Carbon content (wt.%) | Oxygen content (wt.%) |
|---|---|---|---|
| I | 65.7 | 34.3 | 0.0 |
| II | 58.1 | 40.7 | 1.3 |
| III | 64.9 | 32.6 | 2.5 |

As the Co-BTC-powder-derived material is a cobalt/carbon composite material where cobalt and carbon are not homogenously distributed but appear as carbon matrix with embedded cobalt particles, the results differ for different measurement areas on powder particles. They are displayed in ESI-Table 3 to support the results of gravimetric analysis regarding the cobalt and the carbon content. It was demonstrated that the carbon content of the thermolysed powder was determined to be more than three times higher than for the thermolysed Co-BTC film if the same characterisation method is applied.

## Thermal analysis of $[Co_3(BTC)_2(H_2O)_{12}]$ powder

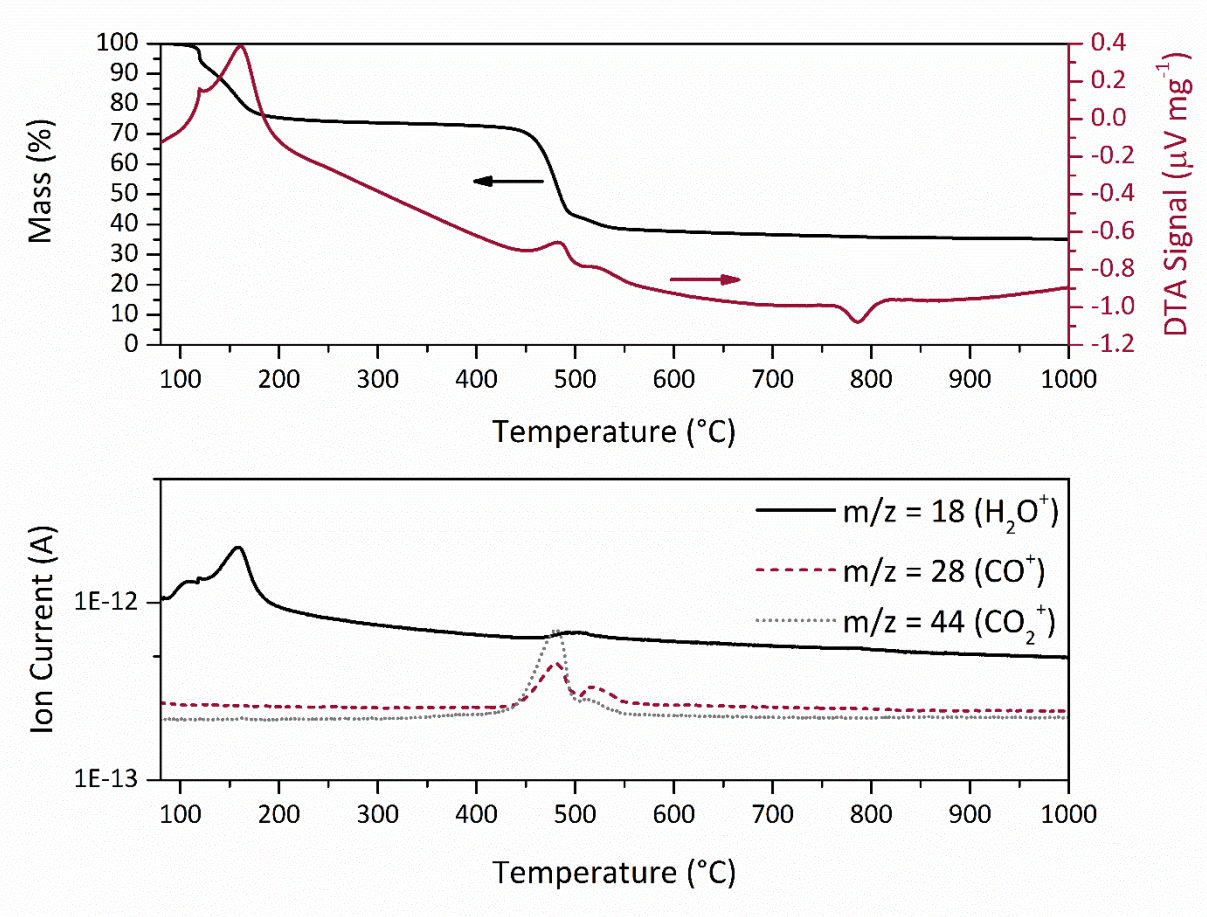


**ESI-Fig. 5** Results of the thermal analysis of electrochemically prepared $[Co_3(BTC)_2(H_2O)_{12}]$ powder under argon atmosphere.

## Electrochemical impedance spectroscopy of MOF-derived electrodes

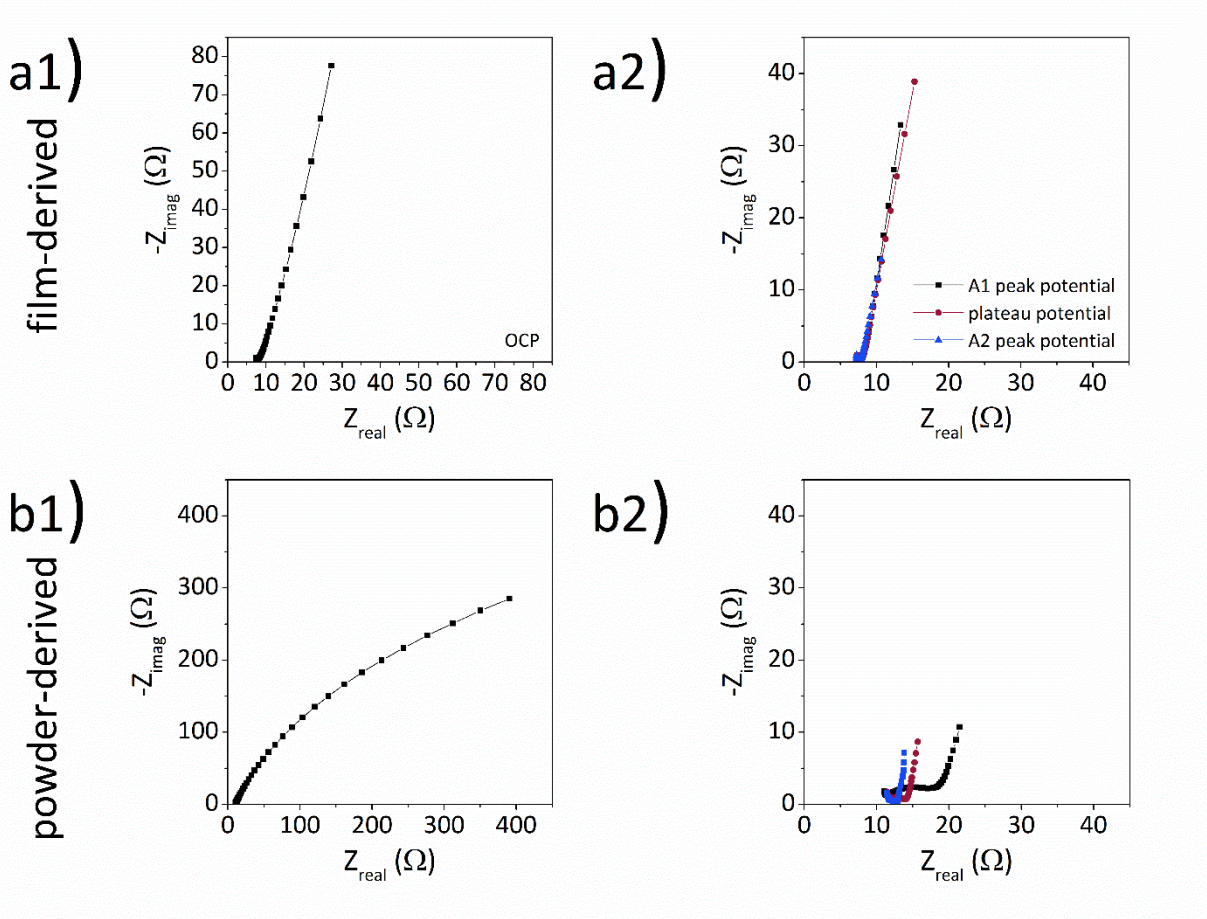


**ESI-Fig. 6** Nyquist plots obtained in a frequency range from 10 kHz to 1 Hz of (a) a Co-BTC film-derived electrode and of (b) a Co-BTC powder-derived electrode in 0.5 M KOH at (a1, b1) open circuit potential and (a2, b2) further potentials related to significant features of the previously measured CVs.

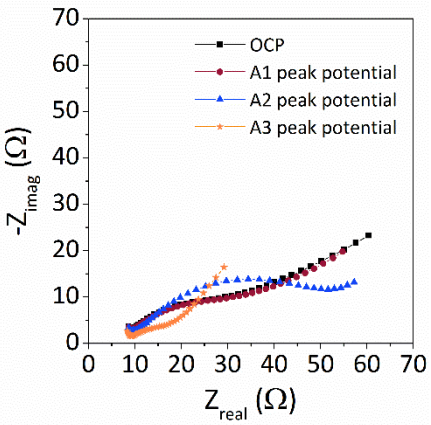


**ESI-Fig. 7** Nyquist plots obtained in a frequency range from 10 kHz to 1 Hz of a Mn/Mn-BTC film-derived electrode in 0.5 M $K_2SO_4$ at open circuit potential and potentials related to significant features of the previously measured CVs.

## References


(1) Pourbaix, M.: *Atlas of Electrochemical Equilibria in Aqueous Solutions*; Pergamon Press: Oxford, New York, 1966.

(2) Vetter, K. J.: *Electrochemical Kinetics*; Academic Press: New York, London, 1967.

(3) Hamann, C. H.; Hamnett, A.; Vielstich, W.: *Electrochemistry*; 2 ed.; WILEY-VCH Verlag GmbH & Co. KGaA: Weinheim, 2007.

(4) Conway, B. E.: *Supercapacitors. Scientific fundamentals and technological applications*; Kluwer Academic: New York, 1999.

(5) Liu, T. C.; Pell, W. G.; Conway, B. E. Stages in the development of thick cobalt oxide films exhibiting reversible redox behavior and pseudocapacitance. *Electrochim. Acta* **1999**, *44*, 2829-2842.

(6) Brousse, T.; Bélanger, D.; Long, J. W. To Be or Not To Be Pseudocapacitive? *J. Electrochem. Soc.* **2015**, *162*, A5185-A5189.

(7) Conway, B. E.; Birss, V.; Wojtowicz, J. The role and utilization of pseudocapacitance for energy storage by supercapacitors. *J. Power Sources* **1997**, *66*, 1-14.

(8) Simon, P.; Gogotsi, Y.; Dunn, B. Where Do Batteries End and Supercapacitors Begin? *Science* **2014**, *343*, 1210-1211.